CrystEngComm

PAPER

View Article Online
View Journal | View Issue

Cite this: *CrystEngComm*, 2024, **26**, 2862

Dazzling $Ca_2LuScAl_2Si_2O_{12}:Ce^{3+}$ green-emitting garnet-type phosphors for blue-chip-pumped white light-emitting diodes: broad emission band, high quantum efficiency and excellent thermal stability

Cheng Xian,[a] Xiaoyuan Chen,[a] Balaji Devakumar[b] and Xiaoyong Huang *[a]

Exploring efficient, energy-saving and environmentally friendly phosphors is important for developing solid-state white light-emitting diodes (w-LEDs). Herein, we report a novel highly efficient green-emitting Ce^{3+}-activated $Ca_2LuScAl_2Si_2O_{12}$ (abbreviated as CLSAS:Ce^{3+}) garnet phosphor with high quantum efficiency and good thermal stability. These garnet phosphor samples doped with different Ce^{3+} ion concentrations were synthesized using a high-temperature solid-state method. The crystal structure and Ce^{3+} concentration-dependent luminescence properties of the phosphors were systematically studied. The as-prepared CLSAS:Ce^{3+} garnet phosphors exhibit broadband absorption in the spectral range of 250–510 nm with a maximum excitation wavelength of around 452 nm, matching well with the emission wavelengths of commercial blue LED chips. Under an excitation of 452 nm, the optimal CLSAS:4%Ce^{3+} sample exhibited a broad green emission band (emission peak: 531 nm; bandwidth: 114 nm) with CIE color coordinates of (0.3293, 0.5453) and high luminescence efficiency (internal quantum efficiency: 87.3%; external quantum efficiency: 56.6%). The CLSAS:4%Ce^{3+} sample also showed good thermal stability in the temperature range of 303–443 K. Its emission intensity at 423 K reached 79% of the emission intensity at 303 K, and it exhibited outstanding color stability with a small color chromaticity shift (ΔE = 1.07 × 10^{-3}) at 423 K. Importantly, the fabricated w-LED device exhibits excellent photoelectric properties (CCT = 4978 K; Ra = 92.4; LE = 69.59 lm W^{-1}). The obtained efficient CLSAS:Ce^{3+} green phosphors have the potential for application in high-quality w-LEDs.

Received 15th March 2024,
Accepted 5th May 2024

DOI: 10.1039/d4ce00258j

rsc.li/crystengcomm

1. Introduction

With the sustainable development of the social economy, excessive energy consumption has always been an important issue.[1–7] Previous reports have shown that about 22% of the electric power in the USA is consumed in the field of lighting.[8] Thus, how to reduce lighting energy consumption has become the research direction of many researchers. Notably, if all the world's traditional white light sources such as incandescent lamps, fluorescent lamps and high-pressure gas discharge lamps were converted to light-emitting diode (LED) light sources, energy consumption could be reduced by about 1000 TW h y^{-1}.[9] Notably, white LEDs (w-LEDs) are expected to bring about a technological revolution in the lighting field and offer the opportunity to replace traditional light sources as the mainstream lighting technology owing to their better photoelectric conversion efficiency, environmental friendliness and long working lifetime.[10–16] The color rendering index (CRI) is a crucial parameter for analyzing the performance of w-LEDs, which indicates the degree of color reduction of an object under artificial and standard (sunlight) light sources. In general, the higher the CRI, the stronger the ability to restore the color of an object. As is well known, the CRI value required for general lighting is greater than 80.[17] Particularly, in some lighting fields requiring high-quality warm white light, including photography, surgery, museums, jewellery, cinematography, and art galleries, the CRI value should be higher than 90.[18,19] Thus, the development of high-CRI w-LEDs is of great significance for high-quality lighting.

At present, the common w-LED devices on the market are made by directly coating yellow phosphor particles (YAG:Ce^{3+}) on blue LED chips.[20–26] Although the human eye recognizes the mixture of blue and yellow light as white light (cold white light), the poor CRI (<75) due to the lack of red spectral components has limited further application in some

[a] *College of Electronic Information and Optical Engineering, Taiyuan University of Technology, Taiyuan 030024, P.R. China. E-mail: huangxy04@126.com*
[b] *Centre for Nanoscience and Nanotechnology, Sathyabama Institute of Science and Technology, Chennai 600119, India*

fields. Thus, to overcome this shortcoming, w-LEDs can be fabricated by combining blue LED chips with green-emitting and red-emitting phosphors.[27–29] Indeed, there are some blue-light-excitable green phosphors reported for w-LEDs applications, but they have many disadvantages. For example, the $SrGa_2S_4:Eu^{2+}$ green phosphor is limited in commercial applications due to the instability of sulfides.[30] The synthesis conditions of β-SiAlON:Eu^{2+} green phosphors are harsh, requiring high temperature and high pressure,[31] leading to higher prices. The thermal stability of the $(Ba,Sr)_2SiO_4:Eu^{2+}$ green phosphor is poor at high temperatures.[32] Consequently, high-performance green phosphors excited by blue light still have great room for development in the field of high-quality warm w-LEDs. Besides, the presence of the cyan gap (in the 480–520 nm spectral range) significantly affects the CRI values of w-LEDs. The introduction of additional cyan-emitting phosphors can improve spectral continuity and make it more comfortable for the human eyes. However, at present, the developed cyan-emitting phosphors still have some problems such as poor stability and low luminescence efficiency, and the addition of cyan-emitting phosphors can also lead to manufacturing complexity and undesirable reabsorption.[33] Thus, developing blue-light-excited broadband green-emitting phosphors with emission spectra covering the cyan gap and green region may be a better choice.[34]

Rare-earth ions are usually used as activators of phosphors, and their emission colors are generally produced by 4f → 4f or 5d → 4f transitions; the 5d → 4f is the spin- and parity-allowed transition and is more efficient.[35–37] The Ce^{3+} ion is a typical activator for LED phosphors because its excitation and emission processes are based on the spin- and parity-allowed 5d ↔ 4f transitions. Since the 5d orbital of the Ce^{3+} ion is in the outer layer, its luminescence behavior and color are greatly affected by the crystal field environment.[38–40] Thus, by selecting the appropriate host lattice, Ce^{3+}-doped phosphors can achieve efficient broadband green emission. As is well known, garnet compounds have been widely studied for the host materials of LED phosphors. The general formula of the garnet structure is $A_3B_2C_3O_{12}$, where A, B and C are symmetrical cations at different positions.[41,42] The cubic crystal structure of the garnet cell has a complex arrangement of different cations. Because of this, garnet-type phosphors are unique in their tunability of luminescence properties by changing the A, B, and C cations. Thus, compounds with the garnet structure are suitable for Ce^{3+} ions as host materials. In the past, many Ce^{3+}-activated garnet-type phosphors with various emission colors have been developed for w-LED applications, such as cyan-green-emitting phosphor $Ca_2La_{1-x}Lu_xHf_2Al_3O_{12}:Ce^{3+}$,[43] and yellow-emitting phosphor $CaGd_2HfSc(AlO_4)_3:Ce^{3+}$.[44] In this work, we report a novel efficient blue-light-excited green phosphor based on the Ce^{3+}-activated $Ca_2LuScAl_2Si_2O_{12}$ (CLSAS) garnet compound. These phosphors doped with various Ce^{3+} concentrations were synthesized by a traditional high-temperature solid-state method, and their crystal structure and luminescence properties have been comprehensively studied. Under blue light excitation at 452 nm, the optimal CLSAS:4%Ce^{3+} phosphor sample exhibits a broadband green emission in the range of 462–750 nm with an emission peak at 531 nm and the full width at half maximum (FWHM) of 114 nm. Notably, the CLSAS:4%Ce^{3+} phosphor has a high internal quantum efficiency (IQE = 87.3%) and excellent thermal stability (the emission intensity at 423 K reached 79% of that at 303 K). A w-LED device with a high CRI value of 92.4 was fabricated by combining the CLSAS:4%Ce^{3+} green phosphor and (Ca,Sr)$AlSiN_3:Eu^{2+}$ commercial red phosphor with a 450 nm blue chip. Overall, our results show that the green-emitting CLSAS:Ce^{3+} phosphors with excellent QE and good thermal stability have great application potential in high-quality w-LED lighting.

2. Experimental procedures

A series of CLSAS:x%Ce^{3+} (x = 1%, 2%, 4%, 6%, 8%) phosphors were synthesized by a conventional high-temperature solid-state reaction. $CaCO_3$ (analytical reagent), Lu_2O_3 (purity of 99.99%), Sc_2O_3 (purity of 99.99%), Al_2O_3 (analytical reagent), SiO_2 (purity of 99%), and $Ce(NO_3)_3{\cdot}6H_2O$ (purity of 99.99%) were used as raw materials and weighed according to the corresponding stoichiometric ratio. The weighed raw materials were placed in an agate mortar for complete grinding, and the well-blended mixtures were collected and placed in a muffle furnace, and calcined at 1400 °C for 6 h in a reducing atmosphere of CO. After the heating procedure, these resulting samples were taken out and thoroughly ground into fine powders for further characterization.

X-ray diffraction (XRD) patterns of the phosphor powders were obtained using a Bruker D8 diffractometer with Cu Kα radiation (λ = 1.5405 Å). Rietveld refinement analysis was performed on the XRD data using the FullProf Suite software. Photoluminescence excitation (PLE) spectra and photoluminescence emission (PL) spectra of the samples at room temperature were obtained using an Edinburgh FS5 spectrometer equipped with a 150 W xenon lamp. The IQE values were measured by the integrating sphere method using the Edinburgh FS5 spectrometer. PL spectra at different temperatures were obtained using an Edinburgh FS5 spectrometer with a temperature controller. Finally, the CIE color coordinates were obtained by importing the PL spectral data into the CIE1931 program.

The CLSAS:4%Ce^{3+} green phosphor was mixed with the (Ca,Sr)$AlSiN_3:Eu^{2+}$ commercial red phosphor and epoxy resin, and then the mixture was coated on a 450 nm blue chip to make a w-LED device. The photoelectric properties of this LED device were measured by an OHSP-350M integrating sphere spectroradiometer system.

3. Results and discussion

The XRD pattern of the CLSAS:4%Ce^{3+} phosphor is shown in Fig. 1(a). All diffraction peaks match well with the $Gd_3Al_5O_{12}$

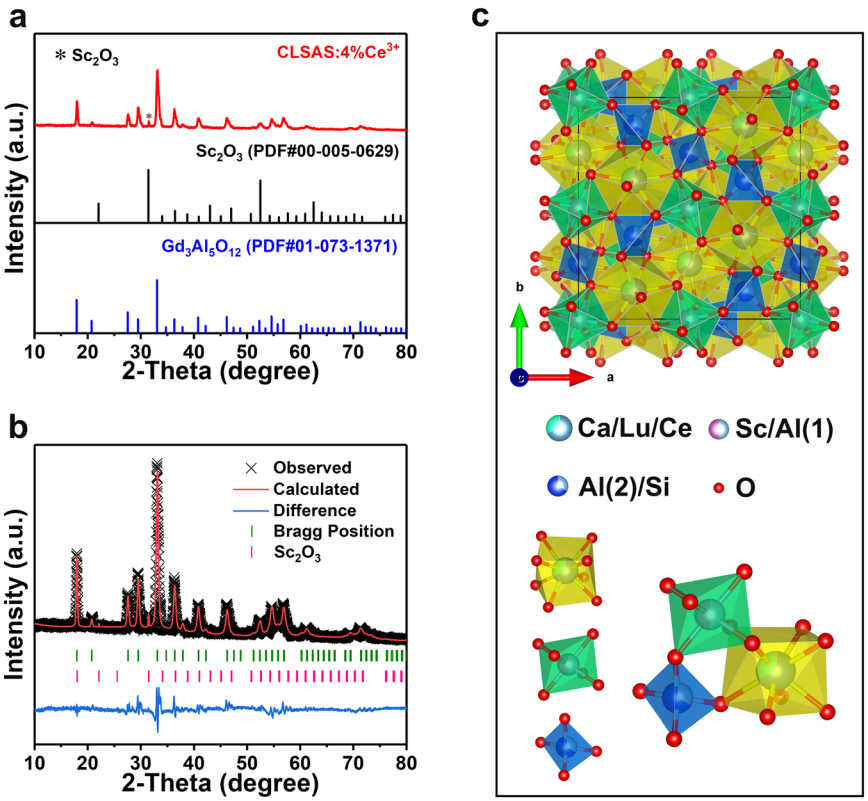

Fig. 1 XRD pattern (a), Rietveld refinement (b), and crystal structure (c) of the CLSAS:4%Ce^{3+} phosphor.

(PDF#01-073-1371) standard card, except for a weak peak at 31.478 degrees due to Sc_2O_3 impurity, indicating that the sample is a garnet cubic system with the $Ia\bar{3}d$ space group. Considering the low impurity ratio (about 2.59 wt%), its effect on the optical properties of the sample is negligible. To obtain detailed structural information, the Rietveld refinement analysis of the XRD pattern of CLSAS:4%Ce^{3+} phosphor was carried out and the results are shown in Fig. 1(b) and Table 1. For a more accurate refinement, the impurity Sc_2O_3 was also introduced as the second phase during the refinement process. The low values of goodness-of-fit (χ^2 = 2.98), *R*-pattern factor (R_{wp} = 7.42%) and weighted profile *R* factor (R_p = 6.98%) show that the refinement is reasonable. The lattice parameters are $\alpha = \beta = \gamma = 90°$, $a = b = c$ = 12.1041 Å and V = 1773.361(0.473) Å^3, which further ensure that the as-prepared sample has the garnet structure. The atomic coordinates of the CLSAS:4%Ce^{3+} phosphor are shown in Table 2.

Fig. 1(c) shows the crystal structure of the CLSAS:4%Ce^{3+} phosphor, in which the coordination environments of the cations are annotated. The Ca and Lu ions occupying the 24c Wyckoff positions are connected to the eight surrounding O^{2-} anions to form a dodecahedron. Considering the same valence state and similar ionic radius, it is assumed that Ce^{3+} (CN = 8, r = 1.143 Å) is more inclined to replace Lu^{3+} (CN = 8, r = 0.977 Å). Besides, Sc/Al(1) and Al(2)/Si occupying 16a and 24d positions are octahedral and tetrahedral coordination, respectively. The octahedron [Sc/Al(1)O_6] and tetrahedron [Al(2)/SiO_4] are connected by O^{2-} ions, which share edges and corners with the dodecahedron [Ca/Lu/CeO_8] to form a three-dimensional crystal structure framework.

The PLE and PL spectra of the CLSAS:4%Ce^{3+} phosphor at room temperature are shown in Fig. 2(a). When 531 nm is used

Table 1 Refined crystal parameters of the CLSAS:4%Ce^{3+} phosphor

Formula	CLSAS:4%Ce^{3+}
Crystal system	Cubic
Space group	$Ia\bar{3}d$
Lattice parameters	$a = b = c$ = 12.1041 Å $\alpha = \beta = \gamma = 90°$
Unit cell volume	V = 1773.361(0.473) Å^3
R_p	6.98%
R_{wp}	7.42%
χ^2	2.98

Table 2 Atomic coordinates of the CLSAS:4%Ce^{3+} phosphor

Atom	*x*	*y*	*z*	Occupancy
Ca	0.125	0.00000	0.25000	0.66667
Lu	0.125	0.00000	0.25000	0.31600
Ce	0.125	0.00000	0.25000	0.01733
Sc	0.00000	0.00000	0.00000	0.50000
Al1	0.00000	0.00000	0.00000	0.50000
Al2	0.37500	0.00000	0.25000	0.33333
Si	0.37500	0.00000	0.25000	0.66667
O	−0.03240	0.05664	0.15152	1.00000

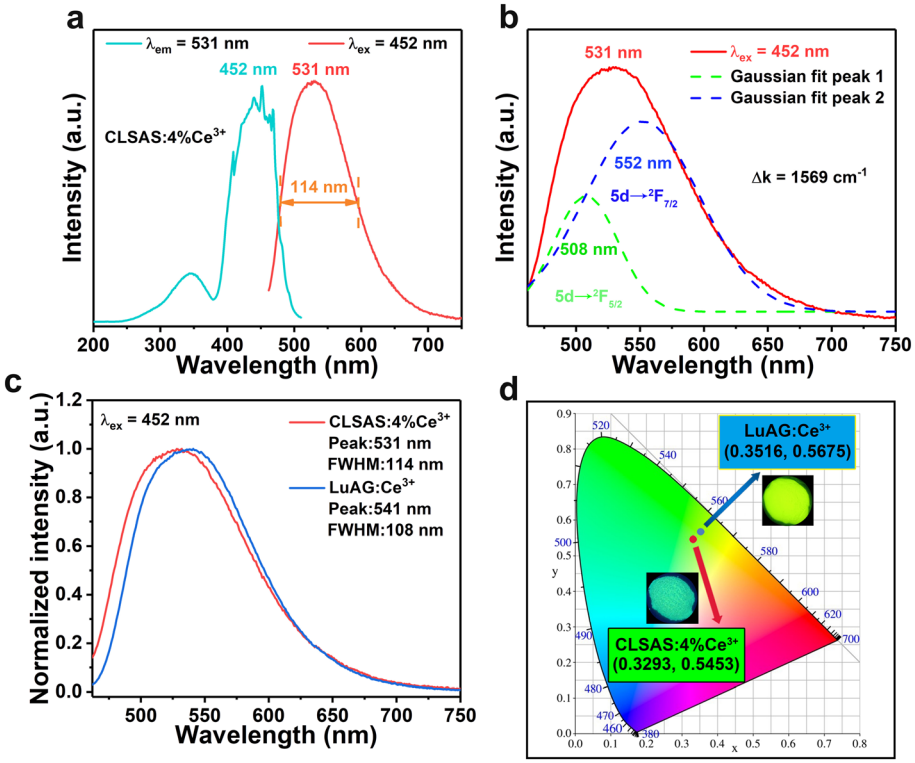

Fig. 2 (a) PLE and PL spectra of the CLSAS:4%Ce^{3+} phosphor. (b) Gaussian fitting PL spectra of the CLSAS:4%Ce^{3+} phosphor. (c) Normalized PL spectra of the as-prepared CLSAS:4%Ce^{3+} phosphor and commercial LuAG:Ce^{3+} green phosphor under 452 nm excitation. (d) CIE chromaticity diagram of the CLSAS:4%Ce^{3+} phosphor and LuAG:Ce^{3+} commercial green phosphor.

as the monitoring wavelength, the obtained PLE spectrum shows a broad absorption band in the 250–510 nm wavelength range, covering the blue and near-ultraviolet regions. The maximum excitation peak is 452 nm, which is related to the 4f → 5d transition of Ce^{3+} ions.[45] Under 452 nm excitation, the emission spectrum shows a broad asymmetric emission band (462–750 nm spectral range) with a peak of 531 nm, covering the cyan gap (480–520 nm) and the green region. In general, the larger the FWHM, the larger the coverage, and the more conducive to manufacturing high-CRI w-LEDs. The FWHM of this CLSAS:4%Ce^{3+} phosphor reached 114 nm, which is larger than that of the $CaSc_2O_4$:Ce^{3+} green phosphor (FWHM = 105 nm).[46] In Fig. 2(b), the asymmetric emission band is decomposed into two sub-bands by Gaussian fitting with peaks at 508 nm and 552 nm, which can be attributed to the radiation transition from the 5d level to the $^2F_{5/2}$ and $^2F_{7/2}$ sub-levels, respectively.[47,48] The energy difference Δk is calculated to be 1569 cm^{-1}, which is close to the theoretical value of 2000 cm^{-1}.[40,49] This result is consistent with the fact that there is only one type of Ce^{3+} luminescence center in the CLSAS host. Fig. 2(c) compares the normalized PL spectra of CLSAS:4%Ce^{3+} green phosphor and commercial LuAG:Ce^{3+} green phosphor under 452 nm excitation. It is observed that CLSAS:4%Ce^{3+} has a wider FWHM than LuAG:Ce^{3+} (114 nm *versus* 108 nm), and the CLSAS:4%Ce^{3+} covers a higher proportion in the cyan gap range (480–520 nm) than LuAG:Ce^{3+}. Fig. 2(d) shows the CIE chromaticity diagram and digital photographs of the as-prepared CLSAS:4%Ce^{3+} green phosphor and the commercial LuAG:Ce^{3+} green phosphor. The CIE color coordinates of the CLSAS:4%Ce^{3+} and LuAG:Ce^{3+} phosphors are determined to be (0.3293, 0.5453) and (0.3516, 0.5675), respectively; and they are located in the green region, which is in good agreement with the illustrations of their emission colors.

To investigate the influence of the Ce^{3+} doping concentration on the optical properties, the PLE and PL spectra of a series of CLSAS:$x$$Ce^{3+}$ (x = 1%, 2%, 4%, 6%, 8%) phosphors are obtained, as shown in Fig. 3(a and b). These phosphor samples show a broad excitation band in the wavelength range of 250–510 nm (see Fig. 3(a)). Among them, the excitation intensity of CLSAS:4%Ce^{3+} phosphor is the strongest, and its excitation peak is located at 452 nm. When excited at 452 nm, these phosphors produce bright green light with emission peaks ranging from 521 nm to 537 nm (see Fig. 3(b)). To further understand the influence of Ce^{3+} concentration on PL properties, the normalized PL spectra of CLSAS:$x$$Ce^{3+}$ phosphors at the same excitation (452 nm) are recorded (see Fig. 3(c)), revealing that their emission peak position undergoes a significant red shift with the increase of Ce^{3+} concentration. The emission peaks, FWHM values and CIE color coordinates of CLSAS:$x$$Ce^{3+}$ phosphors are listed in Table 3. The observed emission red-shift phenomenon can mainly be attributed to the following three reasons. The first reason is that the possibility of energy transfer from the

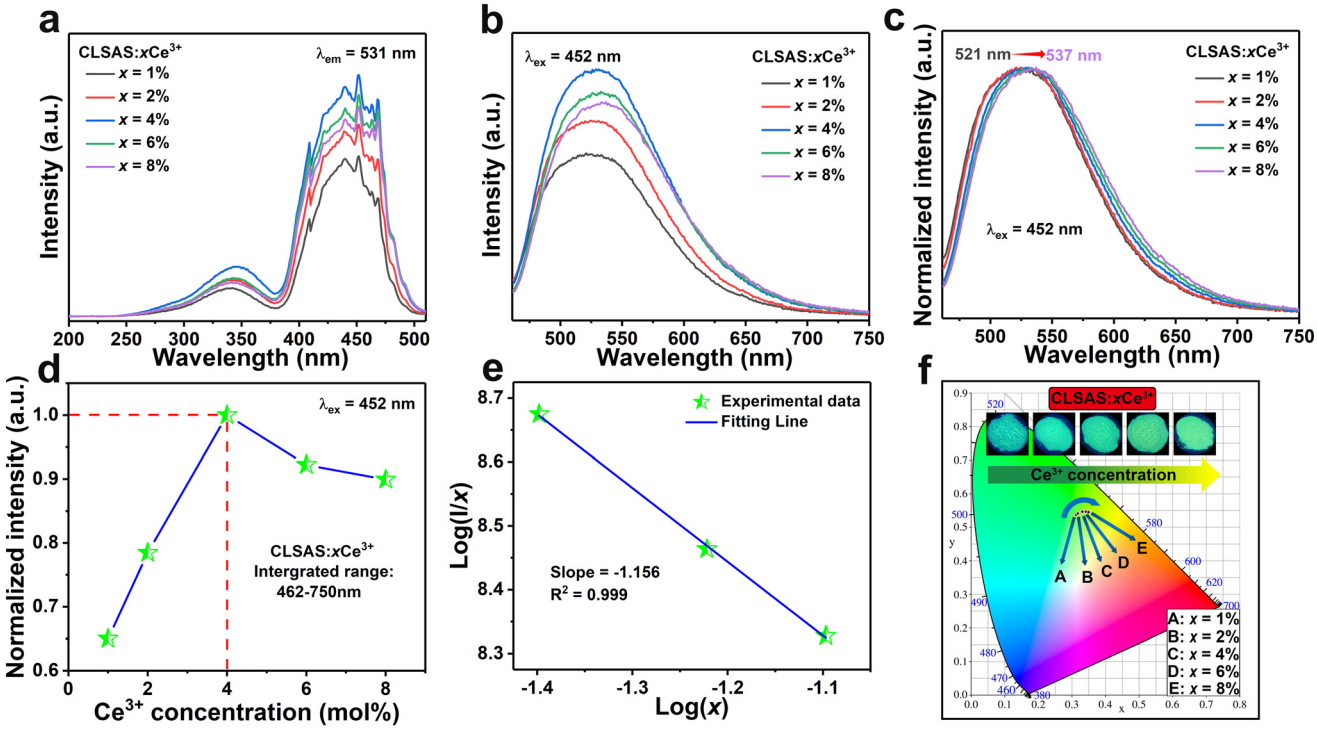

Fig. 3 (a–c) PLE spectra (a), PL spectra (b) and normalized PL spectra (c) of CLSAS:xCe^{3+} (x = 1%, 2%, 4%, 6%, and 8%) phosphors. (d) The relationship between the PL intensity and Ce^{3+} doping concentration. (e) The relationship between log(I/x) and log(x) in CLSAS:xCe^{3+} phosphors. (f) CIE chromaticity coordinates of CLSAS:xCe^{3+} phosphors under 452 nm excitation.

higher energy level to the lower energy level of the Ce^{3+} 5d excited state became greater with the increase of Ce^{3+} concentration, thus reducing the emission of high energy and causing the emission peak to shift towards a larger value. The second reason is related to the crystal field splitting of the 5d orbital,[18] which can be roughly estimated by the following formula:[50,51]

$$D_q = \frac{1}{6} Ze^2 \frac{r^4}{R^5} \quad (1)$$

where D_q is the size of the split energy level, Z is the valence state of the anion, e is the electron charge, r is the radius of the d wave function, and R is the bond length between Ce^{3+} and O^{2-} ions. From the above formula, D_q is proportional to $1/R^5$. For CLSAS:xCe^{3+} phosphors, the larger Ce^{3+} ion (r = 1.143 Å, CN = 8) replaces the smaller Lu^{3+} ion (r = 0.977 Å, CN = 8). Thus, as the concentration of Ce^{3+} increases, the smaller distance between Ce^{3+} ions and O^{2-} will enhance the field strength of the crystal, which in turn leads to a red shift phenomenon in the emission peak. Because there is overlap between PLE and PL spectra, reabsorption may also be responsible for the emission red-shift phenomenon for CLSAS:xCe^{3+} phosphors.[29]

Notably, the PL intensity of CLSAS:xCe^{3+} phosphors increases with the increase in the Ce^{3+} concentration and reaches the maximum at x = 4%. However, when the doping concentration exceeded 4%, the PL intensity begins to decrease (see Fig. 3(d)). This phenomenon is called the concentration quenching effect, which is caused by non-radiative energy transfer between adjacent Ce^{3+} ions.[52,53] Thus, the critical distance R_c is introduced to analyze the energy transfer, and R_c can be approximated by the model proposed by Blasse:

$$R_c = 2\left(\frac{3V}{4\pi x_c N}\right)^{1/3} \quad (2)$$

where V is the unit cell volume, x_c is the critical concentration, and N is the number of available sites of Ce^{3+} in the unit cell. In this formula, V = 1773.361(0.473) Å^3, x_c = 0.04, N = 8, thus the value of R_c is calculated as 21.956 Å. In general, the energy transfer between activators can occur through (i) radiation reabsorption, (ii) exchange interaction, and (iii) electrical multipole interaction.[54,55] Because the calculated R_c value is greater than 5 Å, the exchange interaction is not the mechanism of energy transfer between Ce^{3+} ions. The interaction type can be further analyzed by the following formula:[56–58]

Table 3 Optical parameters of CLSAS:xCe^{3+} phosphors

x	λ_{em} (nm)	FWHM (nm)	CIE (x, y)
1	521	113	(0.3117, 0.5378)
2	525	113	(0.3171, 0.5417)
4	531	114	(0.3293, 0.5453)
6	533	115	(0.3409, 0.5472)
8	537	118	(0.3487, 0.5454)

$$\frac{I}{x} = k\left[1 + \beta(x)^{\theta/3}\right]^{-1} \quad (3)$$

where x denotes the concentration of the activator, I is the emission intensity, and k and β are the host lattice constants under the same emission conditions. The dipole–dipole, dipole–quadrupole, and quadrupole–quadrupole interactions correspond to θ = 6, 8, and 10, respectively. As shown in Fig. 3(e), the slope −1.16 can be obtained by the linear fitting of $\log(I/x)$ and $\log(x)$. Accordingly, the θ value is calculated to be 3.48, which is far less than 6. The overlap of excitation and emission spectra to some extent indicates that radiation reabsorption may also play a role in the energy transfer of CLSAS:xCe^{3+} phosphors.[44] Taken together, the main energy transfer mechanism of Ce^{3+} ions in CLSAS:xCe^{3+} phosphors might be attributed to the combination of electrical multipole interactions and radiation reabsorption.

The PL spectral data are input into the CIE1931 software to calculate the CIE chromaticity coordinates of the CLSAS:xCe^{3+} phosphors with different concentrations. Fig. 3(f) is the CIE chromaticity diagram of the CLSAS:xCe^{3+} samples. As the doping concentration of Ce^{3+} increases from 1% to 8%, their luminescence gradually changes from cyan-green to deep green, and the corresponding CIE chromaticity coordinates also exhibit a red-shift from (0.3117, 0.5378) to (0.3487, 0.5454) (see Table 3).

QE is an important parameter for the performance evaluation of inorganic phosphors in practical applications. The IQE, absorption efficiency (ε) and external QE (EQE) of CLSAS:xCe^{3+} phosphors can be calculated by the following models:[59–61]

$$\mathrm{IQE} = \frac{\int L_S}{\int E_R - \int E_S} \quad (4)$$

$$\varepsilon = \frac{\int E_R - \int E_S}{\int E_R} \quad (5)$$

$$\mathrm{EQE} = \mathrm{IQE} \times \varepsilon \quad (6)$$

where L_S is the emission spectrum of the prepared phosphor; E_S and E_R are the excitation spectra of the integrating sphere with and without the phosphor sample, respectively. Accordingly, the IQE, ε and EQE values of the CLSAS:4%Ce^{3+} phosphor were calculated to be 87.3%, 64.9%, and 56.6%, respectively. This excellent IQE value is higher than those of many other green phosphors, such as $CaSr_2Al_2O_6$:Ce^{3+} (IQE = 31%),[38] $Ca_2LaHf_2GaAl_2O_{12}$:Ce^{3+} (IQE = 40.7%),[62] and $Sr_8CaLu(PO_4)_7$:Eu^{2+} (IQE = 77%).[63]

The thermal stability of phosphors is another important parameter for evaluating LED phosphors. For this purpose, we have studied the luminous stability of the CLSAS:4% Ce^{3+} phosphor at different testing temperatures. Fig. 4(a) shows the temperature-dependent PL spectra of the CLSAS:4%Ce^{3+} phosphor under 452 nm excitation. The emission intensity gradually decreased with the increase in temperature during

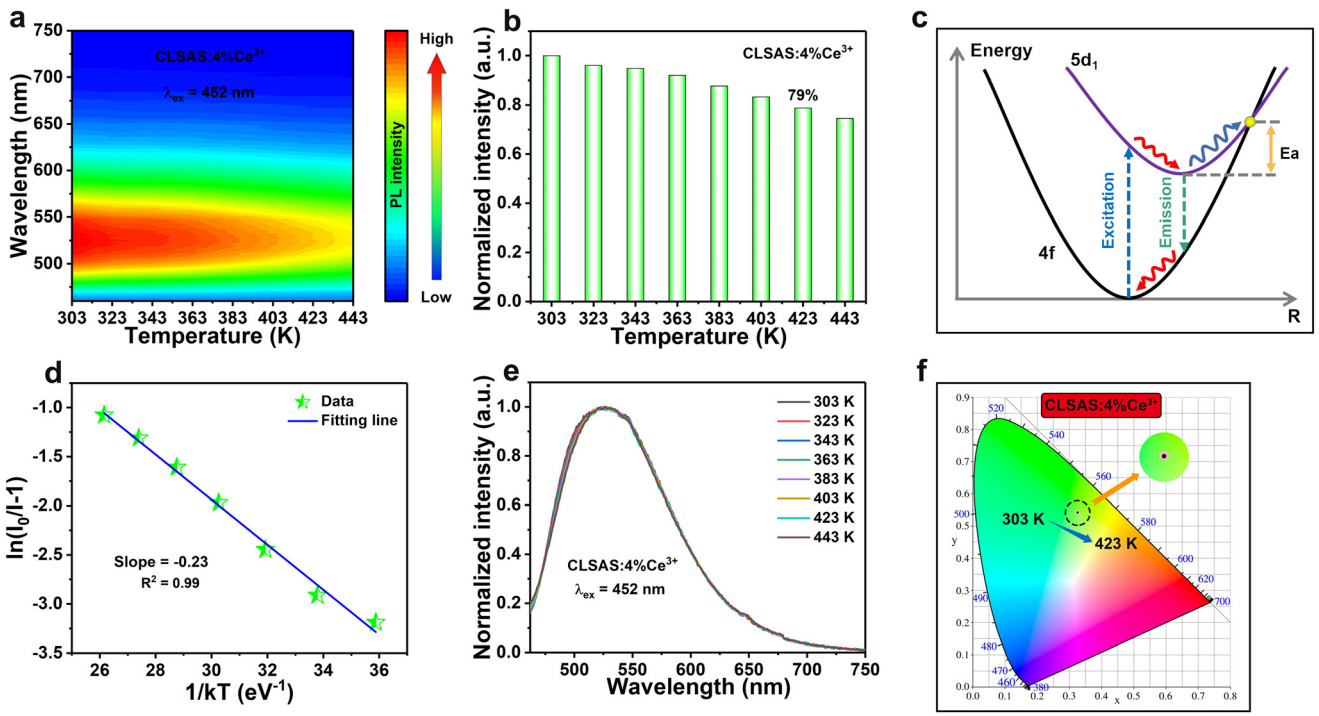

Fig. 4 (a) Temperature-dependent PL spectra of the CLSAS:4%Ce^{3+} phosphor under 452 nm excitation. (b) Normalized PL intensity of the CLSAS:4%Ce^{3+} phosphor at different temperatures. (c) The coordinate configuration diagram of the CLSAS:4%Ce^{3+} phosphor. (d) The fitting diagram of $\ln(I_0/I - 1)$ and $1/kT$. (e) Normalized emission spectra of the CLSAS:4%Ce^{3+} phosphor at different temperatures. (f) CIE chromaticity coordinates of the CLSAS:4%Ce^{3+} phosphor at different temperatures.

Table 4 CIE chromaticity coordinates of the CLSAS:4%Ce^{3+} phosphor at different temperatures

Temperature (K)	CIE (x, y)
303	(0.3241, 0.5435)
323	(0.3245, 0.5437)
343	(0.3253, 0.5437)
363	(0.3260, 0.5439)
383	(0.3257, 0.5438)
403	(0.3256, 0.5438)
423	(0.3255, 0.5432)
443	(0.3253, 0.5428)

heating, indicating that the 5d → 4f transition is greatly affected by temperature, which is caused by thermal quenching.[64] Fig. 4(b) shows that at the operating temperature of 423 K, the emission intensity of the CLSAS:4%Ce^{3+} phosphor reached 79% of the initial intensity at 303 K, which is higher than that of many other green phosphors previously reported, for example, $Ca_2LuHf_2Al_3O_{12}$:Ce^{3+},Tb^{3+} (I_{423K}/I_{303K} = 62%),[65] $Ca_2LaHf_2Al_3O_{12}$:Ce^{3+} (I_{423K}/I_{303K} = 24%),[66] and $Ca_2LaHf_2GaAl_2O_{12}$:Ce^{3+} (I_{423K}/I_{303K} = 20%),[62] suggesting that CLSAS:4%Ce^{3+} has better thermal stability. To better understand the thermal quenching mechanism of the CLSAS:4%Ce^{3+} phosphor, the configuration coordinate model (Fig. 4(c)) is used here to illustrate it. As shown in Fig. 4(c), the electrons absorb heat and then transition to the crossover point, and then return to the ground state through non-radiative transitions.[67] Notably, the distance between the crossing point and the lowest 5d level is the activation energy (E_a). The activation energy (E_a) can also be obtained from the Arrhenius equation:[68,69]

$$\frac{I}{I_0} = \left[1 + C\exp\left(-\frac{E_a}{kT}\right)\right]^{-1} \quad (7)$$

where I_0 and I are emission intensities at room temperature and different temperatures, respectively; C is a constant; and k is Boltzmann's constant. As shown in Fig. 4(d), the experimental data can be well-fitted to a straight line with a slope of −0.23, and thus E_a is 0.23 eV. This activation energy is greater than that of some other Ce^{3+} doped garnet phosphors, such as $Ca_2LaZr_2Ga_3O_{12}$:Ce^{3+} (E_a = 0.203 eV),[70] $Ca_2YZr_2Al_3O_{12}$:Ce^{3+} (E_a = 0.22 eV),[71] indicating that the as-prepared CLSAS:4%Ce^{3+} phosphor is not susceptible to thermal quenching.

To directly study the variation of PL spectra of the CLSAS:4%Ce^{3+} phosphor upon increasing the temperature, its normalized PL spectra at 303–443 K were obtained and shown in Fig. 4(e). It can be seen from the figure that the normalized PL spectra are basically overlapped and the profiles of these emission spectra change slightly with the heating process (from 303 K to 443 K), indicating the excellent color stability of the CLSAS:4%Ce^{3+} phosphor. The CIE chromaticity coordinates of the CLSAS:4%Ce^{3+} phosphor at different temperatures are recorded in Table 4, and all these data are also plotted in the CIE chromaticity diagram (Fig. 4(f)). When the temperature increased from 303 K to 443 K, the CIE color coordinates change from (0.3241, 0.5435) to (0.3253, 0.5428), and these CIE color coordinates almost overlap in the CIE chromaticity diagram. We have also calculated the chromaticity shift (ΔE) by employing the following equation:[72,73]

$$\Delta E = \sqrt{\left(u'_f - u'_i\right)^2 + \left(v'_f - v'_i\right)^2 + \left(w'_f - w'_i\right)^2} \quad (8)$$

where u' = $4x/(3 - 2x + 12y)$, v' = $9y/(3 - 2x + 12y)$, and w' = $1 - v' - u'$; u' and v' are CIE chromaticity coordinates in the uniform color space of $u'v'$; x and y are CIE chromaticity coordinates calculated by the CIE1931 software; i and f represent 303 K and 423 K, respectively. Consequently, chromaticity shift ΔE is calculated as 1.07×10^{-3}, which is much less than that of many other phosphors, such as $CaGd_2HfSc(AlO_4)_3$:Ce^{3+} ($\Delta E = 2.1 \times 10^{-2}$),[44] $CaAlSiN_3$:Eu^{2+} ($\Delta E = 4.4 \times 10^{-2}$),[74] $Ca_2LuHf_2Al_3O_{12}$:Ce^{3+} ($\Delta E = 1.7 \times 10^{-2}$),[75] $CaY_2HfGa(AlO_4)_3$:Ce^{3+} ($\Delta E = 4.05 \times 10^{-3}$).[29] All these results confirm that the CLSAS:4%Ce^{3+} phosphor has exceptional color stability at high temperatures.

To evaluate the application potential of CLSAS:Ce^{3+} phosphors, a w-LED device was fabricated by combining the CLSAS:4%Ce^{3+} green phosphor and the (Ca,Sr)$AlSiN_3$:

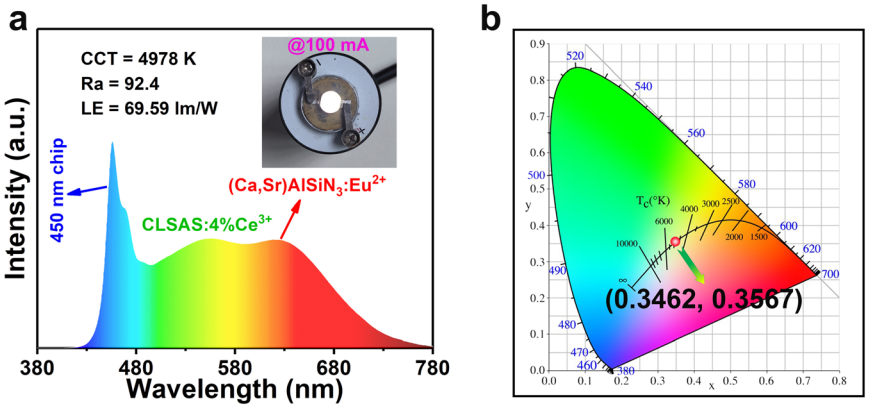

Fig. 5 Emission spectrum (a) and CIE chromaticity diagram (b) of the w-LED device under 100 mA driving current.

Eu^{2+} commercial red phosphor with a 450 nm blue LED chip. Fig. 5(a) shows the emission spectrum of the prepared w-LED under the driving current of 100 mA. The LED device emits bright white light, and the CCT, CRI and LE are 4978 K, 92.4 and 69.59 lm W^{-1}, respectively. The CIE chromaticity coordinates of the w-LED are (0.3462, 0.3567) (see Fig. 5(b)).

4. Conclusion

This work describes the solid-state synthesis and optical properties of green-emitting CLSAS:Ce^{3+} garnet phosphors. Through XRD and Rietveld refinement results, the as-prepared phosphors were found to belong to the cubic crystal system with space group $Ia\bar{3}d$. The CLSAS:Ce^{3+} phosphors have broad absorption bands in the 250–510 nm range with an excitation peak around 452 nm, matching well with the commercial blue LED chips. Under the excitation of 452 nm blue light, the optimal sample CLSAS:4%Ce^{3+} phosphor shows a broadband green emission with a peak at 531 nm and a FWHM of 114 nm, showing an excellent IQE of 87.3% and EQE of 56.6%. Notably, the CLSAS:4%Ce^{3+} green phosphor also exhibits superb thermal stability and color stability. The optimal green phosphor and commercial red phosphor were integrated on a 450 nm blue chip to make a white LED device with excellent photoelectric properties. The CCT, CRI and LE values of the w-LED under a 100 mA driving current are 4978 K, 92.4 and 69.59 lm W^{-1}, respectively. The obtained results show that the CLSAS:Ce^{3+} green phosphor is a promising color converter for application in high-performance w-LEDs.

Conflicts of interest

There are no conflicts to declare.

Acknowledgements

This work was supported by the Fundamental Research Program of Shanxi Province (No. 20210302123153), and the Young Sanjin Scholars Distinguished Professor Program of Shanxi Province.

References

1 S. Zhao, Y. Liu and X. Wu, *CrystEngComm*, 2023, **25**, 1986–1992.
2 A. D. Mahapatra and J.-W. Lee, *CrystEngComm*, 2022, **24**, 7229–7249.
3 P.-Z. Ge, X.-G. Tang, Q.-X. Liu, Y.-P. Jiang and X.-B. Guo, *Energy Mater. Adv.*, 2023, **4**, 0025.
4 A. Chen, X. Li, J. Wang and J. Zhang, *Energy Mater. Adv.*, 2023, **4**, 0028.
5 T. Wang, D. Zhou, Z. Yu, T. Zhou, R. Sun, Y. Wang, X. Sun, Y. Wang, Y. Shao and H. Song, *Energy Mater. Adv.*, 2023, **4**, 0024.
6 Z. Gong, Z. Li, P. Wang, K. Jiang, Z. Bai, K. Zhu, J. Yan, K. Ye, G. Wang, D. Cao and G. Chen, *Energy Mater. Adv.*, 2023, **4**, 0035.
7 F. Lv, Z. Hong, Z. Ahmad, H. Li, Y. Wu and Y. Huang, *Energy Mater. Adv.*, 2023, **4**, 0043.
8 S. Pimputkar, J. S. Speck, S. P. DenBaars and S. Nakamura, *Nat. Photonics*, 2009, **3**, 180–182.
9 M. R. Krames, O. B. Shchekin, R. Mueller-Mach, G. O. Mueller, L. Zhou, G. Harbers and M. G. Craford, *J. Disp. Technol.*, 2007, **3**, 160–175.
10 Y. Q. Li, A. C. A. Delsing, G. de With and H. T. Hintzen, *Chem. Mater.*, 2005, **17**, 3242–3248.
11 A. H. Mueller, M. A. Petruska, M. Achermann, D. J. Werder, E. A. Akhadov, D. D. Koleske, M. A. Hoffbauer and V. I. Klimov, *Nano Lett.*, 2005, **5**, 1039–1044.
12 T. Nishida, T. Ban and N. Kobayashi, *Appl. Phys. Lett.*, 2003, **82**, 3817–3819.
13 X. Huang, *Nat. Photonics*, 2014, **8**, 748–749.
14 X. Huang, *Sci. Bull.*, 2019, **64**, 1649–1651.
15 Z. Jia, C. Yuan, Y. Liu, X.-J. Wang, P. Sun, L. Wang, H. Jiang and J. Jiang, *Light: Sci. Appl.*, 2020, **9**, 86.
16 Q. Yao, P. Hu, P. Sun, M. Liu, R. Dong, K. Chao, Y. Liu, J. Jiang and H. Jiang, *Adv. Mater.*, 2020, **32**, 1907888.
17 X. Huang, S. Wang, B. Li, Q. Sun and H. Guo, *Opt. Lett.*, 2018, **43**, 1307–1310.
18 L. Sun, B. Devakumar, J. Liang, S. Wang, Q. Sun and X. Huang, *J. Mater. Chem. C*, 2020, **8**, 1095–1103.
19 X. Huang, J. Liang, S. Rtimi, B. Devakumar and Z. Zhang, *Chem. Eng. J.*, 2021, **405**, 126950.
20 W. Chen, Y. Cheng, L. Shen, C. Shen, X. Liang and W. Xiang, *J. Alloys Compd.*, 2018, **762**, 688–696.
21 X. Huang, H. Guo, L. Sun, T. Sakthivel and Y. Wu, *J. Alloys Compd.*, 2019, **787**, 865–871.
22 B. Li, G. Annadurai, L. Sun, J. Liang, S. Wang, Q. Sun and X. Huang, *Opt. Lett.*, 2018, **43**, 5138–5141.
23 L. Wang, R.-J. Xie, T. Suehiro, T. Takeda and N. Hirosaki, *Chem. Rev.*, 2018, **118**, 1951–2009.
24 Y. Jin, Y. Hu, H. Wu, H. Duan, L. Chen, Y. Fu, G. Ju, Z. Mu and M. He, *Chem. Eng. J.*, 2016, **288**, 596–607.
25 X. Huang, *Sci. Bull.*, 2019, **64**, 879–880.
26 S. Wang, Q. Sun, B. Devakumar, J. Liang, L. Sun and X. Huang, *RSC Adv.*, 2019, **9**, 3429–3435.
27 X. Ding, Q. Wang and Y. Wang, *Phys. Chem. Chem. Phys.*, 2016, **18**, 8088–8097.
28 M. Liang, J. Xu, Y. Qiang, H. Kang, L. Zhang, J. Chen, C. Liu, X. Luo, Y. Li, J. Zhang, L. Ouyang, W. You and X. Ye, *J. Rare Earths*, 2021, **39**, 1031–1039.
29 J. Chan, L. Cao, W. Li, N. Ma, Z. Xu and X. Huang, *Inorg. Chem.*, 2022, **61**, 6953–6963.
30 Y. H. Kim, P. Arunkumar and W. B. Im, *Ceram. Int.*, 2015, **41**, 5200–5204.
31 S. Li, L. Wang, D. Tang, Y. Cho, X. Liu, X. Zhou, L. Lu, L. Zhang, T. Takeda, N. Hirosaki and R.-J. Xie, *Chem. Mater.*, 2018, **30**, 494–505.
32 L. He, Z. Song, Q. Xiang, Z. Xia and Q. Liu, *J. Lumin.*, 2016, **180**, 163–168.

33 J. Chan, B. Devakumar, W. Li, N. Ma, X. Huang and A. F. Lee, *Appl. Mater. Today*, 2022, **27**, 101439.
34 W. Bai, S. Shi, T. Lin, T. Zhou, T. Xuan and R.-J. Xie, *Adv. Photonics Res.*, 2021, **2**, 2000158.
35 M. Godlewski and M. Leskelä, *Crit. Rev. Solid State Mater. Sci.*, 1994, **19**, 199–239.
36 Z. Xu, B. Devakumar, N. Ma, W. Li and X. Huang, *J. Lumin.*, 2022, **243**, 118640.
37 N. Ma, W. Li and X. Huang, *J. Lumin.*, 2024, **265**, 120232.
38 S. Wang, Q. Sun, B. Devakumar, B. Li, H. Guo and X. Huang, *J. Lumin.*, 2019, **206**, 571–577.
39 N. C. George, J. Brgoch, A. J. Pell, C. Cozzan, A. Jaffe, G. Dantelle, A. Llobet, G. Pintacuda, R. Seshadri and B. F. Chmelka, *Chem. Mater.*, 2017, **29**, 3538–3546.
40 M. Shang, G. Li, D. Geng, D. Yang, X. Kang, Y. Zhang, H. Lian and J. Lin, *J. Phys. Chem. C*, 2012, **116**, 10222–10231.
41 J. Zhong, W. Zhuang, X. Xing, R. Liu, Y. Li, Y. Zheng, Y. Hu and H. Xu, *RSC Adv.*, 2016, **6**, 2155–2161.
42 J. Ueda and S. Tanabe, *Opt. Mater.: X*, 2019, **1**, 100018.
43 J. Chan, L. Cao, Z. Xu and X. Huang, *Mater. Today Phys.*, 2023, **35**, 101130.
44 W. Li, N. Ma, B. Devakumar and X. Huang, *Mater. Today Chem.*, 2022, **23**, 100638.
45 D. Geng, K. Li, H. Lian, M. Shang, Y. Zhang, Z. Wu and J. Lin, *Eur. J. Inorg. Chem.*, 2014, **2014**, 1955–1964.
46 T. Kang, S. Lim, S. Lee, H. Kang, Y. Yu and J. Kim, *Opt. Mater.*, 2019, **98**, 109501.
47 S.-P. Lee, C.-H. Huang, T.-S. Chan and T.-M. Chen, *ACS Appl. Mater. Interfaces*, 2014, **6**, 7260–7267.
48 Z. Sun, Z. Zhu, Z. Guo, Z.-c. Wu, Z. Yang, T. Zhang and X. Zhang, *Ceram. Int.*, 2019, **45**, 7143–7150.
49 W. Zhou, F. Pan, L. Zhou, D. Hou, Y. Huang, Y. Tao and H. Liang, *Inorg. Chem.*, 2016, **55**, 10415–10424.
50 H. Zhang, Y. Chen, X. Zhu, H. Zhou, Y. Yao and X. Li, *J. Lumin.*, 2019, **207**, 477–481.
51 J. Sun, Z. Lian, G. Shen and D. Shen, *RSC Adv.*, 2013, 18395–18405.
52 X. Huang and H. Guo, *Dyes Pigm.*, 2018, **152**, 36–42.
53 Q. Sun, S. Wang, L. Sun, J. Liang, B. Devakumar and X. Huang, *Mater. Today Energy*, 2020, **17**, 100448.
54 J. Liang, L. Sun, B. Devakumar, S. Wang, Q. Sun, H. Guo, B. Li and X. Huang, *RSC Adv.*, 2018, **8**, 27144–27151.
55 J. Liang, L. Sun, B. Devakumar, S. Wang, Q. Sun, H. Guo, B. Li and X. Huang, *RSC Adv.*, 2018, **8**, 31666–31672.
56 X. Zhang, J. Zhang, R. Wang and M. Gong, *J. Am. Ceram. Soc.*, 2010, **93**, 1368–1371.
57 X. Zhang, X. Tang, J. Zhang and M. Gong, *J. Lumin.*, 2010, **130**, 2288–2292.
58 G. Annadurai, M. Jayachandiran, S. M. M. Kennedy and V. Sivakumar, *Mater. Sci. Eng., B*, 2016, **208**, 47–52.
59 Q. Dong, J. Yang, J. Cui, F. Xu, F. Yang, J. Peng, F. Du, X. Ye and S. Yang, *Dalton Trans.*, 2020, 1935–1946.
60 J. Liang, B. Devakumar, L. Sun, Q. Sun, S. Wang and X. Huang, *J. Am. Ceram. Soc.*, 2019, **102**, 4730–4736.
61 H. Chen, H. Lin, Q. Huang, F. Huang, J. Xu, B. Wang, Z. Lin, J. Zhou and Y. Wang, *J. Mater. Chem. C*, 2016, **4**, 2374–2381.
62 X. Huang, Z. Xu and B. Devakumar, *Ceram. Int.*, 2023, 26420–26427.
63 J. Zhou, M. Chen, J. Ding, J. Zhang, J. Chen, D. Wu and Q. Wu, *Ceram. Int.*, 2021, **47**, 31940–31947.
64 L. Cao, W. Li, B. Devakumar, N. Ma, X. Huang and A. F. Lee, *ACS Appl. Mater. Interfaces*, 2022, **14**, 5643–5652.
65 N. Ma, W. Li, B. Devakumar, Z. Zhang and X. Huang, *J. Colloid Interface Sci.*, 2021, **601**, 365–377.
66 J. Liang, L. Sun, S. Wang, Q. Sun, B. Devakumar and X. Huang, *J. Alloys Compd.*, 2020, **836**, 155469.
67 J. Ueda, *J. Ceram. Soc. Jpn.*, 2015, **123**, 1059–1064.
68 Z. Xia, J. Zhou and Z. Mao, *J. Mater. Chem. C*, 2013, 5917–5924.
69 L. Yang, Y. Wan, H. Weng, Y. Huang, C. Chen and H. J. Seo, *J. Phys. D: Appl. Phys.*, 2016, **49**, 325303.
70 J. Zhong, W. Zhuang, X. Xing, R. Liu, Y. Li, Y. Liu and Y. Hu, *J. Phys. Chem. C*, 2015, **119**, 5562–5569.
71 X. Wang and Y. Wang, *J. Phys. Chem. C*, 2015, **119**, 16208–16214.
72 X. Zhang, L. Huang, F. Pan, M. Wu, J. Wang, Y. Chen and Q. Su, *ACS Appl. Mater. Interfaces*, 2014, **6**, 2709–2717.
73 C.-C. Tsai, W.-C. Cheng, J.-K. Chang, L.-Y. Chen, J.-H. Chen, Y.-C. Hsu and W.-H. Cheng, *J. Disp. Technol.*, 2013, **9**, 427–432.
74 L. Huang, Y. Zhu, X. Zhang, R. Zou, F. Pan, J. Wang and M. Wu, *Chem. Mater.*, 2016, **28**, 1495–1502.
75 Z. Zhang, B. Devakumar, S. Wang, L. Sun, N. Ma, W. Li and X. Huang, *Mater. Today Chem.*, 2021, **20**, 100471.

